MATERIALS AND MANUFACTURING PROCESSES, 16(1), 1–16 (2001)

CHARACTERIZATION AND PROPERTIES OF ALUMINUM COMPOSITE MATERIALS PREPARED BY POWDER METALLURGY TECHNIQUES USING CERAMIC SOLID WASTES

L. Ma. Flores-Vélez,[1] J. Chávez,[2] L. Hernández,[3] and O. Domínguez[3]

[1]FCQ-UASLP, Dr. M. Nava 6, CP 78210, San Luis Potosi, SLP, Mexico
[2]IIM-UNAM, Circuito exterior CU, CP 04510, México City, Mexico
[3]IM-UASLP, 550 Sierra Leona CP 78210, San Luis Potosi, SLP, Mexico

ABSTRACT

This work provides preliminary results of aluminum metal matrix composites (MMCs) reinforced with granulated slag (GS) and electric arc furnace dust (EAFD). The present work concerns the synthesis and properties of Al/GS and Al/EAFD composites based on powder metallurgy techniques. The hardness and compressive strength of the sintering compacts were determined to compare the mechanical properties of the composite material as a function of the GS and EAFD content. The best results were obtained with the Al/GS composites, which reached compressive strengths up to 372 MPa.

1.0 INTRODUCTION

At present, metal matrix composites (MMCs) have been developed to a level of commercial production. Potential users of Al-reinforcing particle composites are expected to be the automotive industries. However, the high cost of many of the reinforcing compounds remains as the major barrier in the widespread use of composites in other applications. A possible way to avoid this handicap would

be the employment of particles obtained from the recycling of some industrial solid wastes. This idea is becoming popular and several studies have been done with fly-ash, glass, and other byproducts (1,2).

Two of the major waste products of the steelmaking industry are slag and electric arc furnace dust (EAFD), both of which are generated each year in significant volumes of thousands of tons, giving these byproducts the potential for added value if suitable end products could be produced from these materials. Tighter environmental regulations have prompted industry to search new methods of treating waste by-products generated by electric arc furnace during the manufacture of steel. Slag and dust are generated during the manufacture of steel via the smelting of scrap metal. EAFD is considered a hazardous solid waste because it contains small amounts of Pb, Cr, and Zn oxides which are evaporated at high temperatures above the steel bath and condensed in the off-gas systems. Because of the large quantities of slag and dust produced and the present expensive manner by which it is discarded, new methods for treating and using these solid wastes are required. The use of these solid wastes as reinforcing particles in a metallic matrix is proposed among the possible applications of granulated slag (GS) and EAFD. The present work reports preliminary results concerning the synthesis and mechanical properties of Al/GS and Al/EAFD composites, which have the potential of becoming a low-cost MMC materials.

2.0 EXPERIMENTAL PROCEDURE

Commercially pure (99%) aluminum needles supplied by Sigma-Aldrich were used in this investigation. Slag and EAFD were received from a domestic steelmaking industry. Aluminum needles and slag were mechanically ground using a ball-milling drum. Aluminum powder, GS, and EAFD were mixed using a rotating drum blender. Hexane was incorporated during the aluminum milling process to reduce oxidation.

The oxide and the phase compositions of the aluminum, slag, and EAFD were determined by X-ray diffraction (XRD) and energy dispersive X-ray spectroscopy (EDX). The final mean size of Al particles was about 55 μm, and particles had a flake-like morphology (Figure 1). On the other hand, slag particles were irregular with a mean particle size of 35 μm (Figure 2a). The major components in the GS were CaO, SiO_2 and FeO, with variable amounts of MgO, Al_2O_3 and MnO (Figure 2b). Figure 3a shows that the EAFD was determined as franklinite ($ZnO \cdot Fe_2O_3$) and cincite (ZnO), with some small amount of hematite (Fe_2O_3). The size, distribution, and shape of the powder particles were evaluated using scanning and transmission electron microscopy (SEM and TEM, respectively). The EAFD contained small amounts of Pb, Cu, Si, and As oxides (Figure 4a) and was mainly composed of nanometric spherical particles with diameter below 300 nm (Figure 4b). From conventional picnometry, the GS presented a mean apparent density of 3.2 $g \cdot cm^{-3}$ and the EAFD of 4.1 $g \cdot cm^{-3}$.

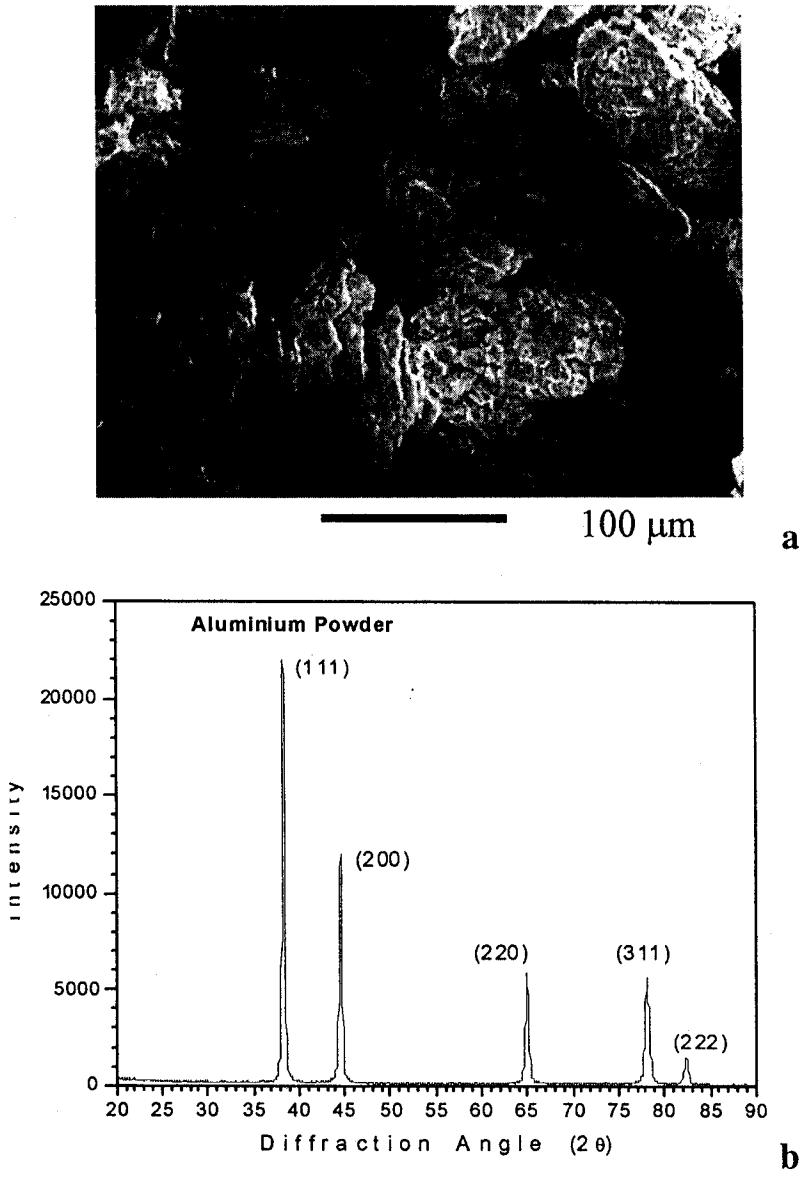

Figure 1. Scanning electron microscopy image (a) and X-ray diffraction (b) obtained from aluminum powder.

Al/GS and Al/EAFD composites were manufactured by conventional uniaxial compaction and sintering powder metallurgy techniques. Table 1 shows the different Al/GS and Al/EAFD mixtures that were prepared. The powder mixtures were compacted in air at room temperature at pressures ranging from 150 to 600 MPa. The compacts prepared were then sintered in Ar atmospheres up to 620°C, using in all cases a heating rate of 10°C/min. The soaking time at the final temperature ranged from 0 to 1 hr. The green density of compacts was determined by picnometry as a function of the compacting pressure and GS or EAFD composition. Densification during sintering of green compacts was also evaluated as a

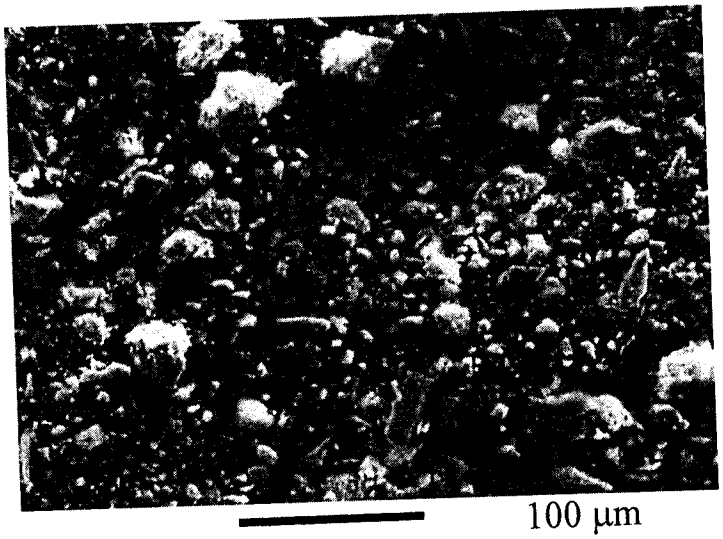

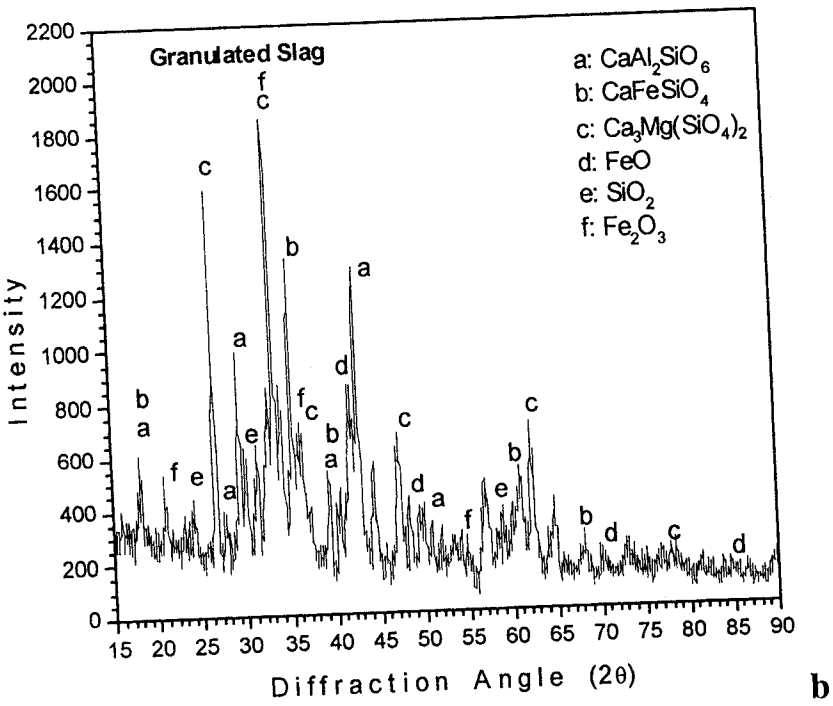

Figure 2. Scanning electron microscopy image (a) and X-ray diffraction (b) obtained from granulated slag.

function of increasing slag and dust content using dilatometric techniques. Hardness and compressive strength of the sintering compacts were determined in order to compare the mechanical properties of the composite material as a function of the EAFD and GS content. Compressive testing was performed under displacement control using an Instrom 20 kN screw-driven machine. Five-cylindrical shaped specimens of each blend were used with a diameter of 4 mm and a length of 8 mm, using in all cases a constant cross-head speed of 0.76 mm · min^{-1}.

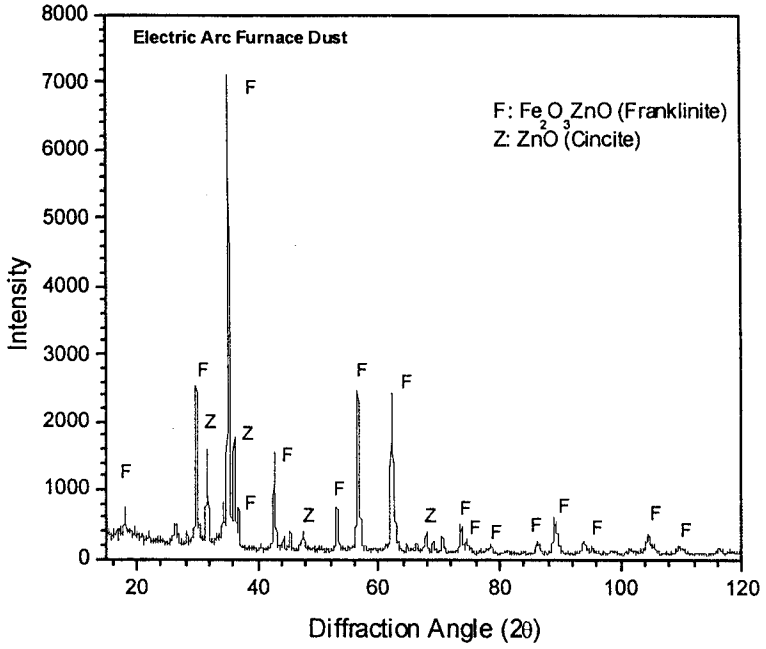

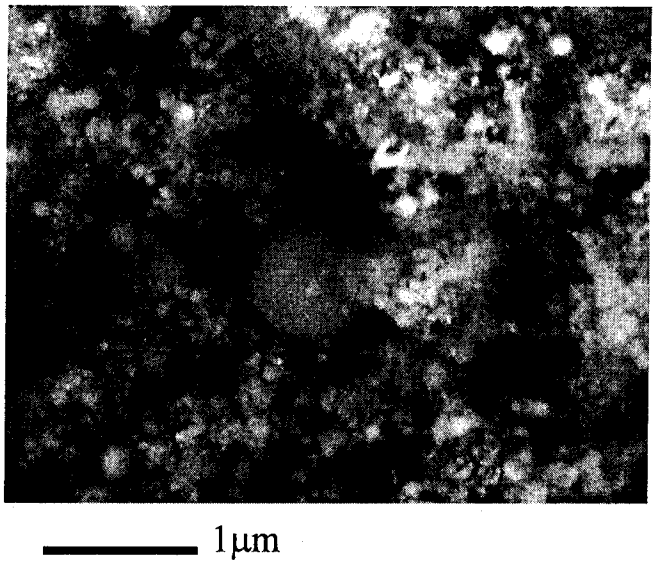

Figure 3. X-ray diffraction (a) and scanning electron microscopy image (b) obtained from the electric arc furnace dust.

3.0 RESULTS AND DISCUSSION

The predominant goal in powder compaction is to achieve good compact properties with minimal applied force. Particle packing is important in most powder-forming processes, because the packing density dictates the die fill, binder content, and shrinkage in sintering. Increasing pressure during compaction provides better packing (via particle rearrangement and plastic deformation) and leads to decreasing porosity with the formation of new particle contacts (3). Figure 5

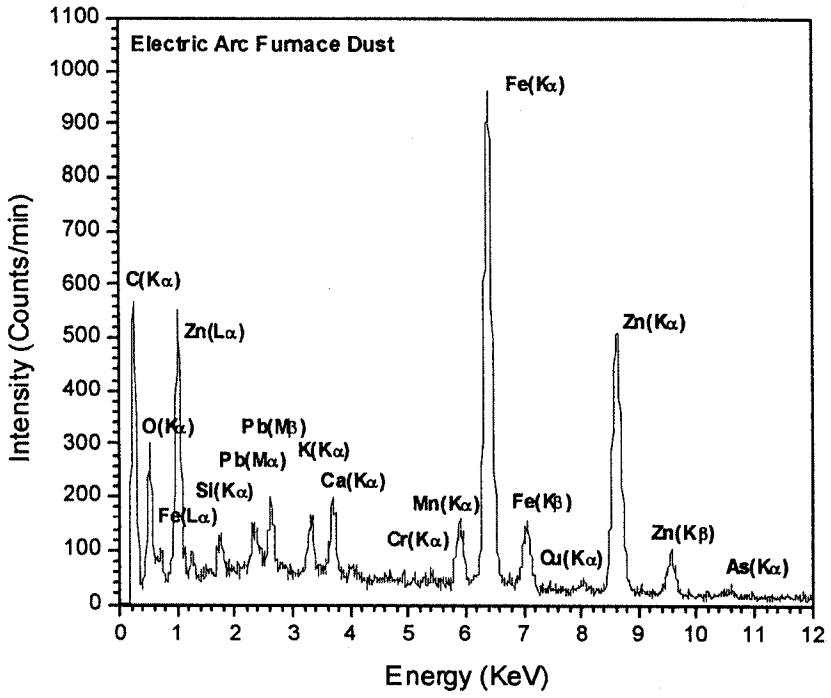

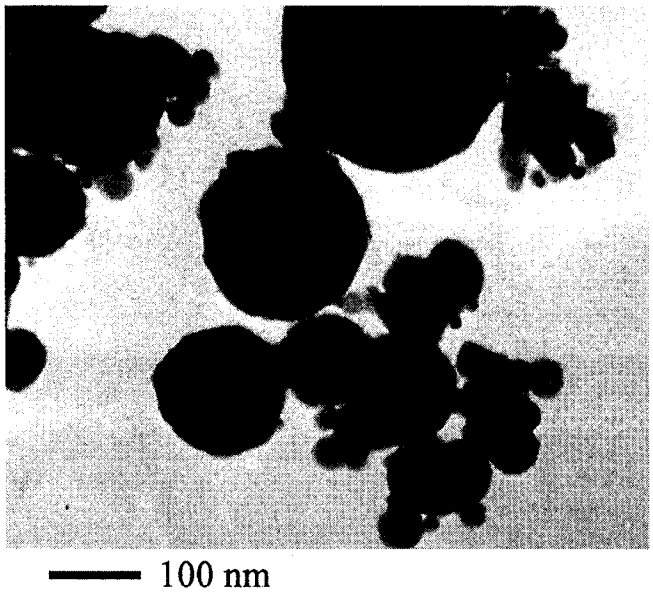

Figure 4. Energy dispersive X-ray spectroscopy (a) and transmission electron microscopy image (b) obtained from the electric arc furnace dust.

shows the effect of compaction pressure on Al powders, indicating that the sample density increases with increasing pressure, approaching relative densities of 98% at 600 MPa. The same procedure was carried out with the mixtures of Al and each of the industrial ceramic particles. For Al/GS, the presence of the slag particles inhibited densification (Fig. 5), where a density of only 90% in the 85Al15GS

Table 1. Chemical Composition (wt %) of the Prepared Composites

Designation	Aluminum	Granulated Slug	EAF Dust
95Al5EAFD	95		5
90Al10EAFD	90		10
80Al20EAFD	80		20
95Al5GS	95	5	
85Al15GS	85	15	
75Al25GS	75	25	
65Al35GS	65	35	

material was produced at highest compaction pressure. The bulk density of both composites, Al/GS and Al/EAFD, was calculated according to the rule-of-mixture (4) where the relative density corresponds to the ratio between compact density and theoretical density.

Powder metallurgy manufacturing experience has shown that green density of compacts depends on several parameters such as particle morphology, chemical composition, surface area, mean particle size, and particle size distribution. Green density usually decreases with decreasing particle size (3) and compaction of pow-

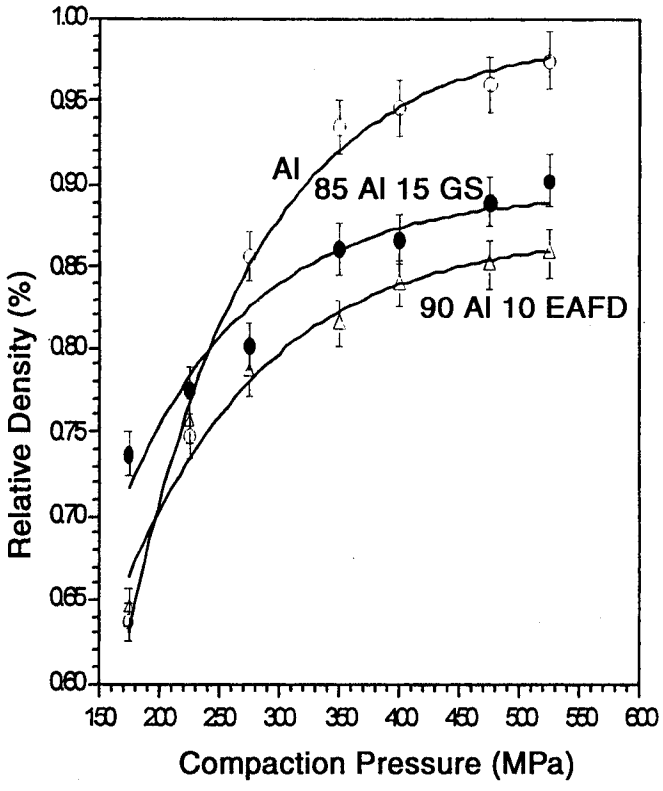

Figure 5. Relative density versus compaction pressure of samples during Al, Al/GS, and Al/EAFD powder consolidation.

ders becomes quite difficult when particles belong to the nanometric domain (5,6). As the TEM image illustrates in Figure 4, the EAFD is basically composed of particles in the nanometric range. Figure 5 shows the effect of compaction pressure on Al/EAFD powders, indicating that 10% of EAFD particles reduce densification more than 15% of GS particles. Therefore, the presence of the extremely fine ceramic particles inhibited densification more, and a relative density of only 85% in the 90Al10EAFD material was achieved at the highest pressure, illustrating the problems associated to the MMC materials produced by powder metallurgy techniques (Fig. 5). Other experimental studies have found that densification of metallic powders is always easier than the densification of the powder mixtures (7). Similar results were obtained for the other volume fractions of GS and EAFD. Figure 5 indicates that above 400 MPa the gain in densification in Al/GS and Al/EAFD compacts was quite small, hence all the compacts subjected to sintering were compacted at this pressure.

During dilatometry, all experiments were carried out at a constant heating rate of 10°C/min. Relative shrinkage ($\Delta L/L_0$) was calculated as the change in sample length divided by its initial length. Figure 6 shows results obtained by dilatometry from samples having different GS content. From these experiments, it was observed that shrinkage in Al/GS composites starts at 175°C. After sintering the samples to 620°C, the compact density measured at room temperature changes from 93 to 98% for pure Al and from 86 to 90% for those having 15 wt % of GS. These curves indicate that during constant heating rate sintering, the final density of compacts is affected by the slag content on the sample, specially once

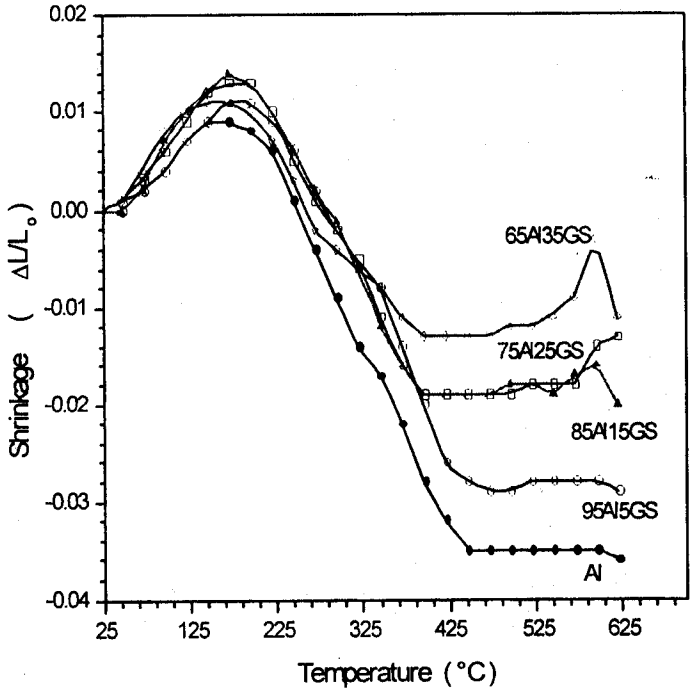

Figure 6. Sintering curves of the Al/GS composites as a function of slag content. All samples compacted to 400 MPa.

the GS content exceeds 25 wt %. In addition, the presence of peaks on the dilatometric curves (Fig. 6) could indicate not only a difference of thermal expansion coefficients between the matrix and the particles, but also the presence of other phenomena such as phase changes, release of trapped gas, and oxidation.

On the basis of thermodynamic considerations, there is the possibility of chemical reactions between the aluminum powder and the constituents of the GS and EAFD, such as SiO_2, ZnO, and FeO. In sufficient quantity, certain alloying elements can form intermetallic compounds with the aluminum and appear as second-phase precipitates in the samples. Such interfacial reactions between the metal and the reinforcement particles would influence the properties of the composite. The possible chemical reactions between the aluminum powder and the constituents of the solid wastes used in this study are shown as follows (8):

$$3/2\ FeO\ (s) + Al\ (s) = 1/2\ Al_2O_3\ (s) + 3/2\ Fe \qquad \Delta G^0(873\ K) = -389.78\ kJ \tag{1}$$

$$3/2\ ZnO\ (s) + Al\ (s) = 1/2\ Al_2O_3\ (s) + 3/2\ Zn\ (l) \qquad \Delta G^0(873\ K) = -308.1\ kJ \tag{2}$$

$$3/4\ SiO_2\ (s) + Al\ (s) = 1/2\ Al_2O_3\ (s) + 3/4\ Si\ (s) \qquad \Delta G^0(873\ K) = -136.40\ kJ \tag{3}$$

At the experimental temperature of 620°C, the Gibbs free energy changes in these chemical reactions are negative, indicating the possibility of chemical reactions between the aluminum powder and the reinforcement particles. Nevertheless, free energy changes can only tell if reactions are plausible and only the kinetics of the solid-state reactions will dictate the occurrence of such processes. To increase the densification of MMC blends and observe the possible occurrence of reactions during sintering, different soaking times at 620°C were carried out. The best results were obtained using a thermal treatment of 1 hr at this temperature. SEM images of Al/GS composites heated to 620°C and held for 1 hr are shown in Figure 7. The typical microstructure of low GS content composite (95Al5GS) shows low porosity levels and relative uniform distribution of the GS (Fig. 7a). Nevertheless, clustering of the particles was observed (Fig. 7c) in the microstructure together with porosity at high slag contents (65Al35GS). After heat treatment, samples with higher concentrations of GS (85Al15GS and 65Al35GS) contained microstructure with slag particles together with another kind of particle having needle-like morphology (Fig. 7b, c, and d). EDX analysis suggests the formation of an Al-Fe intermetallic compound. In general, the slag coming from the steelmaking industry always contains small amounts of iron, so the peak observed on the dilatometric curves at 590°C (Fig. 6) could be associated to the formation of the $FeAl_3$ intermetallic compound as a product of the reaction (9):

$$1/3\ Fe\ (s) + Al\ (s) = 1/3\ FeAl_3\ (s) \qquad \Delta G^0(873\ K) = -57.6\ kJ \tag{4}$$

where the Gibbs free energy change in this chemical reaction was calculated using rough approximations (8,9).

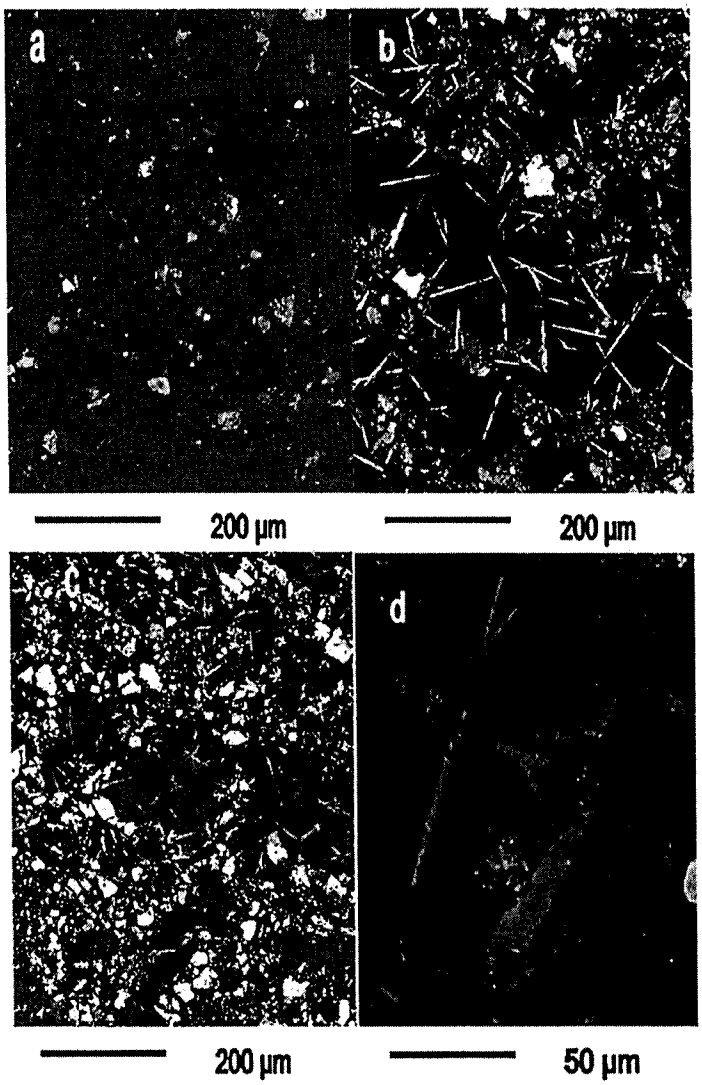

Figure 7. SEM images showing typical microstructures in Al/GS sintered for 1 h at 620°C. (a) 95Al5GS; (b) 85Al15GS; (c) 65Al35GS; and (d) enlargement of precipitates observed in 85Al15GS.

According to thermodynamic analysis, it is likely that silica or zinc and iron oxides were reduced by aluminum powder. Nevertheless, EDX analysis was unable to detect the presence of zinc or silicon in the aluminum matrix. Diffusive mass transport takes place when there is a gradient in the chemical potential and when the species in question has sufficient mobility. The diffusion coefficient of Fe in Al can be approximately estimated to 10^{-9} $cm^2 \cdot sec^{-1}$ at 620° C (10), and those for the corresponding diffusion of the cationic species in the oxide lattice can be estimated in the range of 10^{-15}–10^{-10} $cm^2 \cdot sec^{-1}$ at the same temperature (11). Then, because of the employed experimental conditions and according to diffusional information, if reduction takes place in the solid state, it should be in the metal–solid waste interface. Experimental evidence indicates that there is progressive reduction of silica and iron oxide when processing for longer times above the melting temperature of aluminum (12). Nevertheless, these preliminary

results suggest that during the solid-state sintering process, the fastest reaction concerns the interaction between metallic iron and aluminum powder, producing the needle-like intermetallic precipitate observed on the Al/GS composites.

On the other hand, the results obtained from samples having different EAFD content were different. In this case, the nanometric particles largely affect the sintering behavior and consequently the final density of the composites (Fig. 8). At low EAFD content, it was observed that shrinkage also starts at 175°C. As the EAFD content increased from 5 to 10 wt %, the composite compact expanded drastically. After sintering at 620°C, the compact density at room temperature changed from 82 to 78% for those composites with 20 wt % of EAFD. Once again, thermodynamics indicates the possibility of chemical reaction between the aluminum powder and the EAFD particles, basically by Eq. (2) together with the reaction:

$$1/2\ Fe_2O_3\ (s) + Al\ (s) = 1/2\ Al_2O_3\ (s) + Fe\ (s) \qquad \Delta G^0(873\ K) = -404.7\ kJ \tag{5}$$

where the Gibbs free energy change in this case at 620°C is also negative. The peak observed on the dilatometric curves at 570°C (Fig. 8) could also be associated with the formation of the intermetallic compound as a consequence of reactions (4) and (3), i.e., iron oxide reduction followed by aluminum–iron reaction. Nevertheless, in this case the presence of the intermetallic compound was never observed.

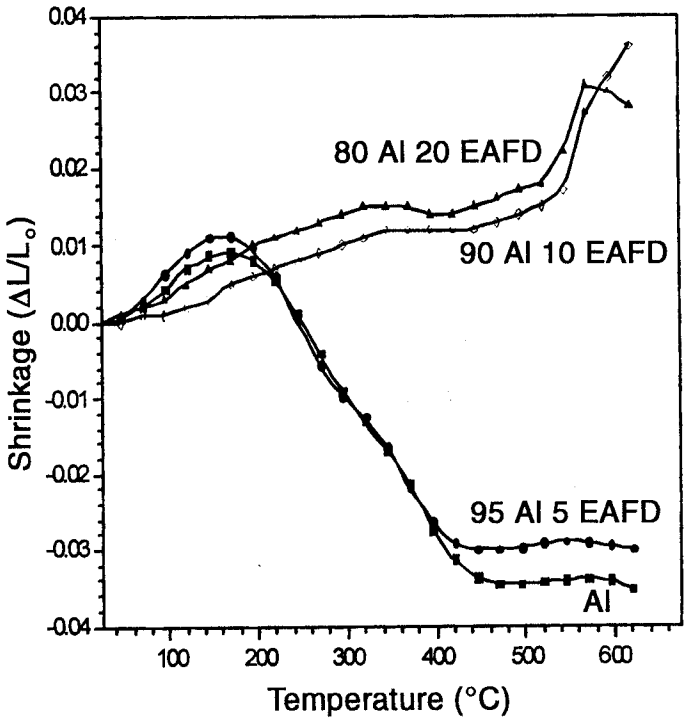

Figure 8. Sintering curves of the Al/EAFD composites as a function of slag content. All samples were compacted to 400 MPa.

SEM images corresponding to the Al/EAFD composites sintered to 620°C and kept for 1 hr at the final temperature are shown in Figure 9. These images illustrate the microstructure of the Al/EAFD composites, revealing moderate porosity levels and no uniform distribution of the particles (Figure 9a) at low EAFD content (95Al5EAFD). At higher EAFD content there is an increase in porosity (90Al10EAFD and 80Al20EAFD), whereas particle distribution seems to be relatively uniform (Fig. 9b and c). However, at large magnification, the uniform distribution comes from agglomeration of the nanometric particles around coarse particles (Fig. 9d).

Agglomeration poses special problems, making compaction and sintering more difficult (8), and probably in the present experimental conditions, particle

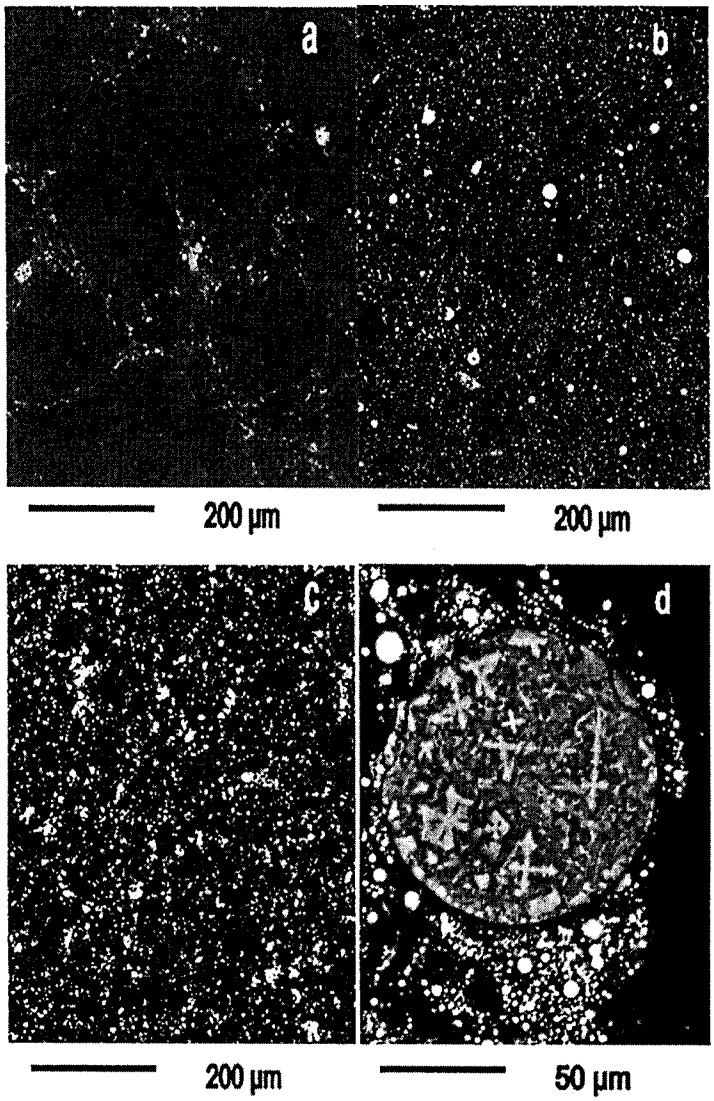

Figure 9. SEM images showing typical microstructures in Al/EAFD sintered for 1 h at 620°C. (a) 95Al5EAFD; (b) 90Al10EAFD; (c) 80Al20 EAFD; and (d) enlargement of agglomerated particles observed in 80Al20EAFD.

agglomeration comes from the as-prepared powders as a consequence of the poor surface-active agent employed during the blending process of Al and EAFD raw powders. Moreover, in the Al/EAFD materials, EDX analysis was unable to detect the presence of needle-like precipitates or the presence of alloying elements in the aluminum matrix. If chemical reactions actually take place in these Al/EAFD composite materials, it should be in the nanoscale metal–solid waste interface. More studies will have to be undertaken, in particular concerning diffusional experiments at the interface of Al/solid–waste particles to discern the possible chemical reaction kinetics involved during processing.

In powder metallurgy all mechanical properties, including strength, elastic modulus, fatigue life and fracture toughness, depend on the sintered density (3,13). Also, the mechanical properties of particulate MMCs are sensitive to the distribution of reinforcing particles (14,15). Inhomogeneity, especially concentrated clusters of particles, is expected to have an adverse effect on the ductility and fracture toughness. Figure 10 shows Vickers hardness as a function of the GS and EAFD content. This figure shows that increasing the amount of GS or EAFD to about 10 and 15% respectively, can result in a considerable increase in the MMC hardness. Beyond these limits, increasing the ceramic particle content weakens the material. In Fig. 10, an important aspect is the hardness peak displacement observed at a lower content of EAFD, probably due to agglomeration and porosity.

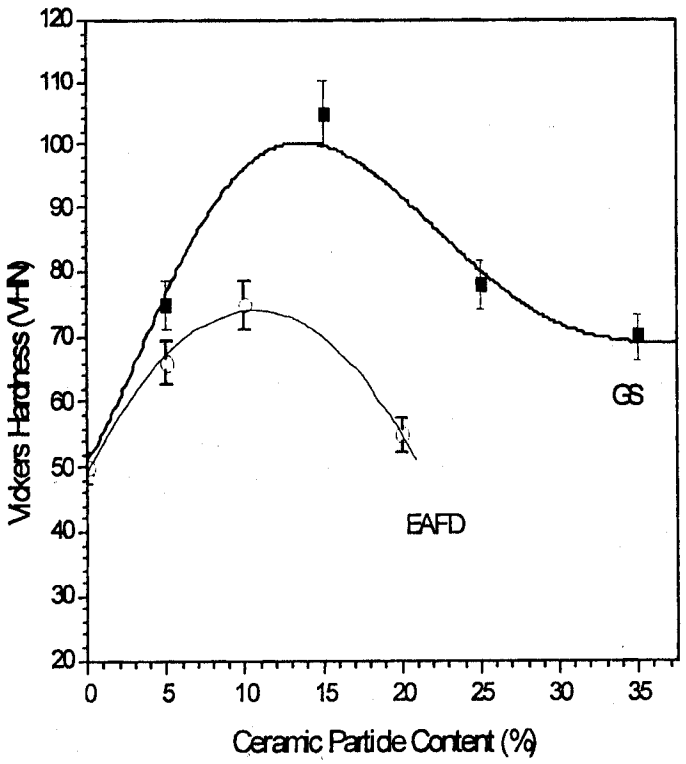

Figure 10. Effect of the ceramic particle content on the composite hardness. Samples were compacted at 400 MPa and sintered at 620°C for 1 hr.

Regarding the mechanical response of the MMCs, Figures 11 and 12 show the typical compression stress–strain curves of the Al/GS and Al/EAFD composites compacted at 400 MPa, then heated to 620°C and held for 60 min. The compressive strength of the Al/GS composites (Figure 11) is relatively high compared to the compressive strength obtained for pure Al (173 MPa). Following the hardness results (Figure 10), the maximum compressive strength was obtained with a GS content corresponding to 15 wt %. The high compressive strength observed could be an indication of good interfacial bonding between the slag particles and the aluminum matrix in Al/GS composites. Another possible mechanism could be the presence of the Al-Fe intermetallic compounds produced during the heat treatment of composites (Figure 7). In the present case, the compressive strength of the MMCs made with 15% GS reached a value of 372 MPa. Once more, the mechanical behavior of the Al/EAFD composites was inferior to that observed using GS. Nevertheless, a compressive strength of 248 MPa was reached with 10% of EAFD (Figure 12). The effect of the ceramic particles on the strength of MMCs is shown in Figure 13. This figure clearly indicates that under the present conditions, the addition of GS and EAFD can increase the compressive strength of the MMCs. Although GS performance is quite better than that of EAFD, the nature of the present discontinuous reinforcement seems to enable an improvement in mechanical properties over the unreinforced matrix. The challenge in the future will be to improve the engineering properties of discontinuously reinforced MMCs via casting processing, making them valuable at a competitive cost compared to their unreinforced counterparts.

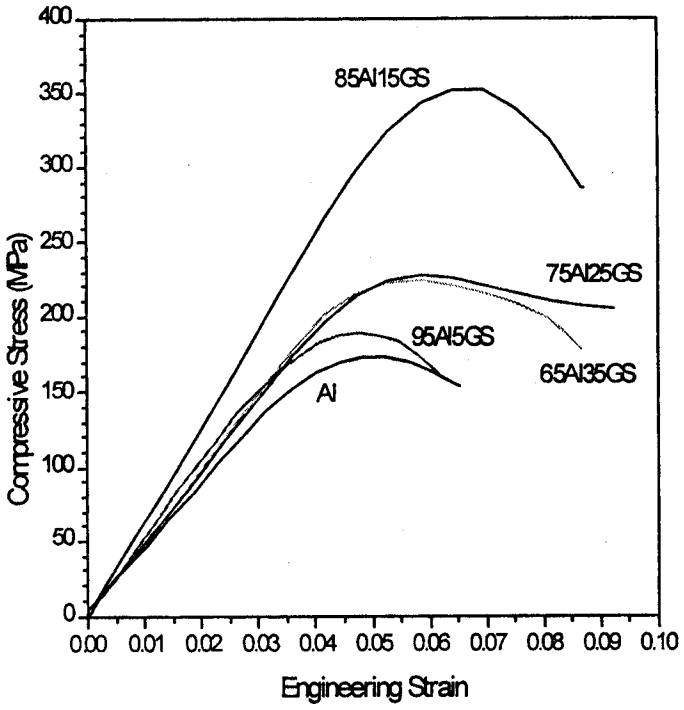

Figure 11. Effect of the GS on the compressive behavior of the sintered Al composites. Samples were compacted at 400 MPa and sintered at 620°C for 1 hr.

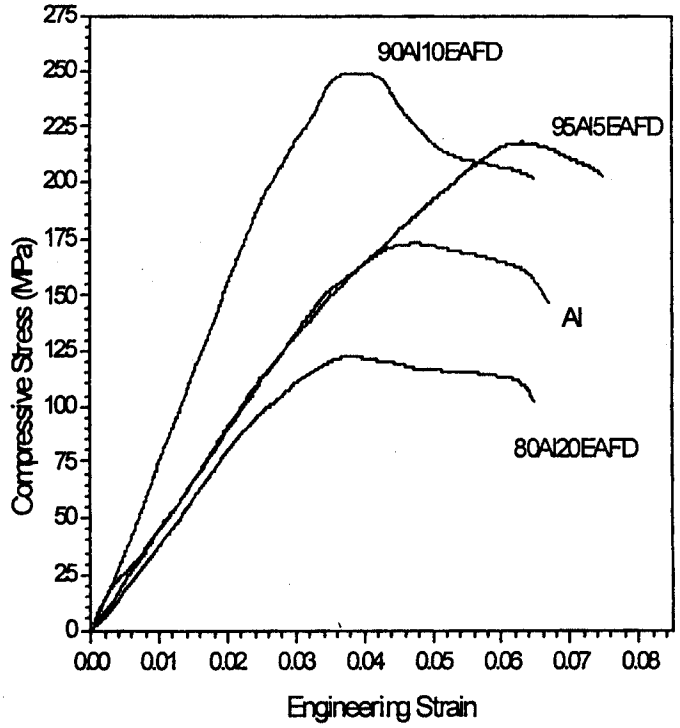

Figure 12. Effect of the EAFD on the compressive behavior of the sintered Al composites. Samples were compacted at 400 MPa and sintered at 620°C for 1 hr.

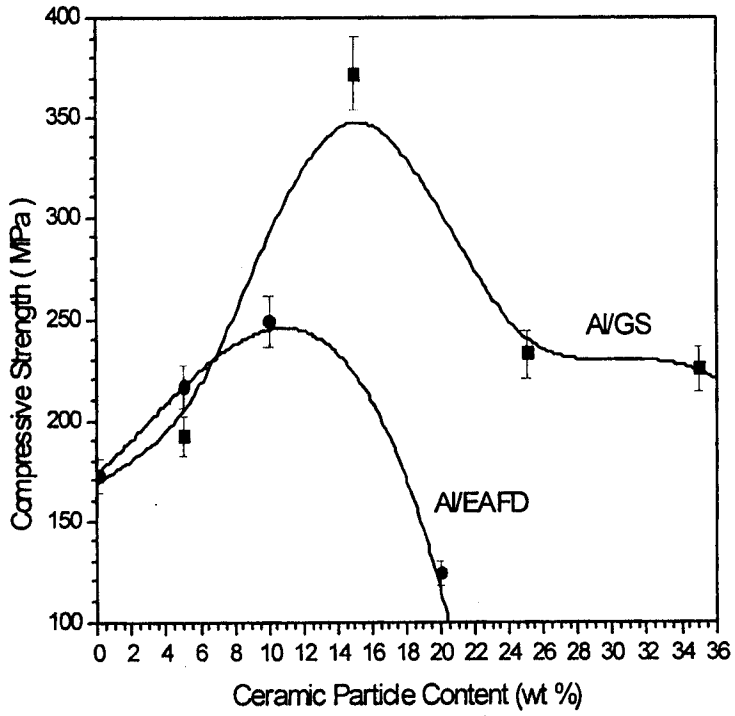

Figure 13. Effect of ceramic particle content on the compressive strength of sintered compacts.

4.0 CONCLUSIONS

The present results indicate that MMCs made of Al/GS and Al/EAFD can be prepared by pressing and sintering techniques involving conventional powder metallurgy processing. The green and sintered densities of the MMCs here obtained were low, ranging from 2.9 to about 3.1 g cm^{-3}. The mechanical response of the Al/GS and Al/EAFD composites was determined in compression. The highest compressive strength of the MMCs made with 15% GS was 372 MPa, and for those made with 10% EAFD the value was 248 MPa. The nature of the present discontinuous reinforcement seems to produce an improvement in mechanical properties over the unreinforced aluminum matrix.

5.0 REFERENCES

1. Rohatgi, P.K.; Guo, R.Q.; Huang, P.; Ray, S. Friction and Abrasion Resistance of Cast Aluminum Alloy-Fly Ash Composites. Metall. Mater. Trans. A **1997**, *28*, 245–250.
2. Domínguez, O. Mexican Patent, pending.
3. German, R.M., *Powder Metallurgy Science*, 2nd Ed.; Metal Powder Industry Federation, 1994.
4. Meyers, M.A.; Chawla, K.K. *Mechanical Behavior of Materials*; Prentice Hall: New York, 1999.
5. Domínguez, O.; Phillipot, J.; Bigot, J. The Relationship Between Consolidation Behavior and Particle Size in Fe Nanometric Powders. Scr. Metall. Mater. **1995**, *32*, 13–15.
6. Andrievski, R.A. Compaction and Sintering of Ultrafine Powders. Int. J. Powder Metall. **1994**, *30*, 59–64.
7. Delie, F.; Bouvard, D. Effect of Inclusion Morphology on the Densification of Powder Composites. Acta Metall. Mater. **1998**, *46*, 3905–3913.
8. Kubaschewski, O.; Alcock, C.B. *Metallurgical Thermochemistry*, 5th Ed.; Pergamon: Elmsford, NY, 1979.
9. Hultgren, R.; Orr, R.L.; Anderson, P.D.; Kelly, K.K. *Selected Values of Thermodynamic Properties of Metals and Alloys*; John Wiley: New York, 1963.
10. Weast, R.C.; Astle, M.J. *CRC Handbook of Chemistry and Physics*, 63rd Ed.; CRC: Boca Ration, FL, 1982.
11. Chiang, Y.M.; Birnie, D.; Kingery, W.D. *Physical Ceramics*; John Wiley: New York, 1997.
12. Guo, R.Q.; Rohatgi, P.K. Chemical Reactions Between Aluminum and Fly Ash During Synthesis and Reheating of Al-Fly Ash Composites. Metall. Mater. Trans. B **1998**, *29*, 519–525.
13. German, R.M. *Sintering Theory and Practice*; John Wiley: New York, 1996.
14. Murphy A.M.; Howard, S.J.; Clyne, T.W. Characterization of Severity of Particle Clustering and Its Effect on Fracture of Particulate MMC. Mater. Sci. Technol. **1998**, *14*, 959–968.
15. Lewandoski, J.J.; Liu, C.; Hunt, W.H. Effect of Matrix Microstructure and Particle Distribution on Fracture of an Aluminum Metal Matrix Composite. Mater. Sci. Eng. **1989**, *A107*, 241–255.